ORGANIC CHEMISTRY FRONTIERS

RESEARCH ARTICLE

View Article Online
View Journal | View Issue

Cite this: *Org. Chem. Front.*, 2021, **8**, 2970

Corannulene-based nanographene containing helical motifs†

Qi Xu,‡[a] Chu Wang,‡[a] Jing He,[a] Xiaonan Li,[a] Ying Wang,[a] Xuebo Chen,[a] Di Sun[b] and Hua Jiang*[a]

Received 10th March 2021,
Accepted 30th March 2021

DOI: 10.1039/d1qo00366f

rsc.li/frontiers-organic

The synthesis and structural analyses of corannulene-PAH hybrids **1** with a [4] helicene subunit and **2** with a [7] helicene subunit have been reported. The structures of **1** and **2** were confirmed by single-crystal X-ray diffraction. The experimental data in combination with theoretical calculations revealed that the terminal ring of helicene and the π-surface of the corannulene unit of **2** adopt a *convex* conformation, which is a more stable conformation. Meanwhile, **2** displays a red-shift in fluorescence emission but a shorter fluorescence lifetime, in comparison with **1**. The optical resolution of **2** was successfully carried out by chiral HPLC, offering enantiopure **P-2** and **M-2**, which were further characterized by CD and CPL spectroscopy.

Introduction

Distorted polycyclic aromatic hydrocarbons (PAHs) or nanographene bearing curved π-conjugated structures have received significant attention due to their unique optical and electronic properties that result from their contorted structures, making them attractive for applications in materials science.[1] Corannulene ($C_{20}H_{10}$), a segment of C_{60}, is regarded as an ideal precursor for developing π-extended distorted PAHs or nanographenes because it has been mass-producible[2] and exhibits distinguishing features that involve *convex*/*concave* π-surfaces, unusual reactivity, thermodynamic bowl-to-bowl inversion, and electron-accepting ability.[3] Thus, tremendous effort has been devoted to discover new features and applications of π-extended distorted PAHs based on the curved structure of corannulene.[4] Consequently, a variety of distorted PAHs or nanographenes fused with corannulene have been developed, and they exhibit potential applications not only in semiconductor materials[5] as organic field-effect transistors and light-emitting devices, but also in bioimaging[6] as potential fluorescent probes. However, there are only limited studies on the chirality of these corannulene-based PAHs or nanographenes.[4c,7] For example, Siegel and Baldridge groups disclosed the indenocorannulene chirality owing to the *concave*/*convex* π-surface of the corannulene unit.[8] Sygula and co-workers developed a corannulene cyclotrimer with three [5] helicene subunits and three corannulene units, which displayed chirality and uncovered the influence of the [5] helicene subunits on the bowl-to-bowl inversion barrier.[7a] Recently, Scott and co-workers synthesized a corannulene-[6] helicene and revealed the effect of concave/convex π-surfaces on the dynamics of the [6] helicene moiety.[4c] More recently, we have also reported helical hybrids of corannulene and dibenzocoronene, which exhibit achiral properties due to the formation of *meso*-double helicenes.[9] These findings demonstrate that the incorporation of helical motifs and corannulene into a fused chiral π-system may produce appealing properties,[4c,7] such as crystal packing, and photophysical and electronic properties. Thus, we were motivated to develop two corannulene-PAH hybrids **1** and **2** bearing different helical lengths (Fig. 1) as models to shed light on the influence of the helical π-system on their properties. We anticipated that the different lengths of the helical motif would significantly change the molecule behaviour and consequently exert great influence on the properties of distorted nanographenes.

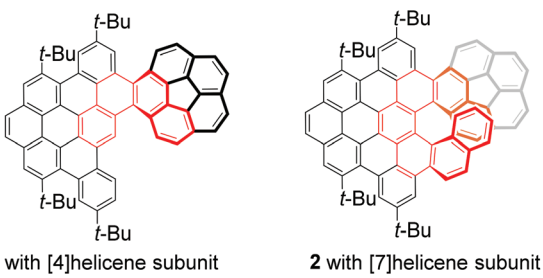

1 with [4]helicene subunit **2** with [7]helicene subunit

Fig. 1 Molecular structures of **1** and **2**.

[a]*College of Chemistry, Beijing Normal University, Beijing 100875, China. E-mail: jiangh@bnu.edu.cn*
[b]*School of Chemistry and Chemical Engineering, Shandong University, Jinan 250100, China*

†Electronic supplementary information (ESI) available. CCDC 1976758, 1976760 and 1976761. For ESI and crystallographic data in CIF or other electronic format see DOI: 10.1039/d1qo00366f

‡These authors contributed equally.

In this work, we report a straightforward bottom-up synthesis of two corannulene–PAH hybrids **1** and **2** with [4] and [7] helicene subunits, respectively (Fig. 1). The structures of **1** and **2** were unambiguously confirmed by X-ray diffraction crystallography and they exhibited different packing motifs in solid phases. The absorption and emission spectra in combination with theoretical calculations revealed the structural diversity and dynamic behaviors. Moreover, owing to the stability of the [7] helicene subunit, two enantiomers of **2** were obtained by chiral HPLC, and their circular dichroism (CD) and circularly polarized luminescence (CPL) spectra were recorded.

Results and discussion

The synthesis of **1** is shown in Scheme 1a. First, cyclopentadienone **3**[9] and ethynylcorannulene **4**[10] undergo the Diels–Alder reaction to afford the intermediate compound **5** in 65% yield. Then, the Scholl reaction of **5** with DDQ as an oxidant resulted in **1** in a good yield of 88% under strongly acidic conditions ($MeSO_3H$) at 0 °C for 1 hour.

The synthesis of **2** is shown in Scheme 1b. In the beginning, palladium-catalyzed Suzuki–Miyaura coupling reaction of **6**[9] and 1-naphthylboronic ester **7**[11] gave a product **8** in 71% yield. Similarly, **8** was further treated with a combination of DDQ and $MeSO_3H$, yielding the desired **2** in 38% yield. The decrease in the yield of **2** can be attributed to the greater steric congestion during the formation of the [7] helicene subunit in comparison with **1** containing a short helical motif. All compounds are characterized by HRMS and NMR spectroscopy (see the ESI†).

The structures of compounds **1**, **2** and **5** in solid phases were unequivocally investigated by single-crystal X-ray diffraction (Fig. 2, Fig. S1–3 and Tables S1–3†). As shown in Fig. 2a and c, the crystal structures indicated that the nanographenes **1** and **2** are hybrids of the planar PAH domain and corannulene unit. The PAH domain was slightly twisted due to the repulsion between the PAH domain and the corannulene unit, leading to the formation of [4] helicene and [7] helicene subunits for **1** and **2** (labelled in blue in Fig. 2a and c), respectively. The dihedral angles of the [4] helicene subunit in **1** and the [7] helicene subunit in **2** calculated from the four inner carbon atoms are 37° and 41° (Fig. S10 and 11†), respectively. Meanwhile, for the [7] helicene subunit in **2**, the centroid–centroid distance of the overlapping terminal rings is 4.10 Å, which is longer than that of the pristine [7] carbohelicene (3.80 Å),[12] presumably due to the convex π-surface of the corannulene unit in **2**. In the corannulene unit, the bowl depths of **1** and **2** are 0.87 Å (Fig. S2c and S3c†), which is the same as that of the parent corannulene (0.87 Å).[13] This observation indi-

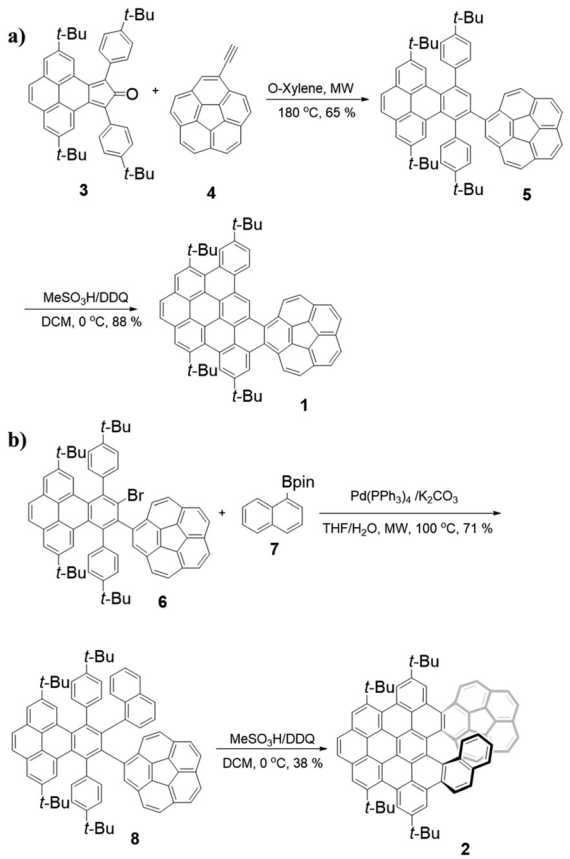

Scheme 1 Synthetic routes of **1** (a) and **2** (b).

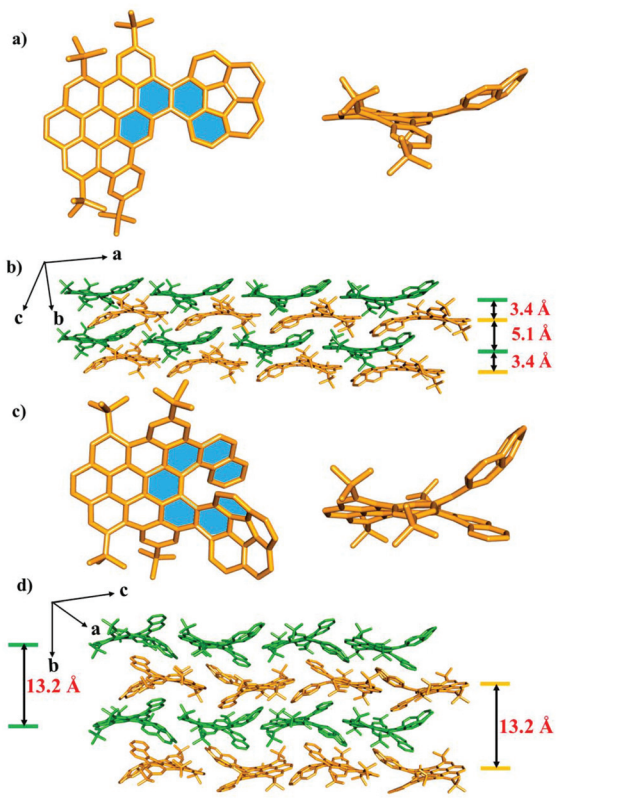

Fig. 2 X-ray crystal structures of the obtained molecules. **1** (a) and **2** (c) from the top and side views. Molecular packing of **1** (b) and **2** (d). Hydrogen atoms are omitted for clarity.

cates that the fusion of PAH and corannulene has no effect on the bowl-depth of the corannulene unit. Importantly, in the case of **1**, two nanographenes display a dimer-like stacking of an antiparallel orientation, which leads to a plane-convex π–π interaction between the planar PAH domain and the corannulene unit with a distance of 3.40 Å (Fig. 2b and Fig. S5†). The propagation of such an antiparallel dimer-like stacking along the crystallographic *a* axis leads to the formation of a double-layer, in which the corannulene units are arranged in a head-to-end layered fashion and display uniform directions. However, the propagation of the double-layer along the crystallographic *b* axis results in bowl-openings to bowl-opening stackings with a distance of 5.1 Å (Fig. 2b and Fig. S5†). In the case of **2**, the nanographenes also adopt a head-to-end layered orientation along the crystallographic *c* axis. However, the bowl-openings of the corannulene units display an alternate upside-down orientation along the crystallographic *c* axis (Fig. 2d). Additionally, in the adjacent layers along the crystallographic *b* axis, two molecules display stackings of antiparallel orientation in which the bowl-openings of the corannulene units show a uniform direction. The average distances (6.6 Å) of the adjacent layers of **2** are the same and completely different from those of **1**. Such observations are ascribed to different steric hindrances that originate from the different lengths of the sub-helical units in the nanographenes **1** and **2** (Fig. 2d).

Thanks to the unique bowl shape of corannulene, one expects that the terminal ring of helicene would face either the *convex* or *concave* π-surface of the bowl if the helical subunit is long enough. In fact, only the *convex* conformation was observed in the solid phase of **2** as demonstrated by X-ray crystallography (Fig. 2). To further shed light on the dynamic behaviours of **1** and **2**, DFT calculations at the B3LYP/6-31G(d) level were performed on both the *convex* and *concave* forms of **1** and **2**. DFT calculations displayed substantial disparities between the thermodynamic stabilities of the *convex* and *concave* conformations (Fig. S19 and 20†). Compared with *concave*-**1** and *concave*-**2**, *convex*-**1** and *convex*-**2** are more stable by 3.2 kcal mol^{-1} (Fig. 3a) and 6.2 kcal mol^{-1} (Fig. 3b), respectively, clearly demonstrating that the *convex* form is the more stable conformation. For **1** and **2**, these results indicate that the *concave* conformations are subjected to larger steric congestion than the *convex* conformations. Furthermore, barriers for bowl-to-bowl inversions from the *convex* to *concave* conformation were estimated to be 11.2 (Fig. S19†) and 11.8 (Fig. S20†) kcal mol^{-1} for **1** and **2**, respectively. These values are very close to that for the pristine corannulene (11.5 kcal mol^{-1}),[13,14] and these results further confirm the negligible steric influence of the bowl-to-bowl inversions. They also suggest that fast interconversions between the *convex* and *concave* conformations can occur in solution but the *convex* conformations predominate as demonstrated in the solid state. A similar phenomenon has been reported by Scott and co-workers.[4c]

Next, the photophysical properties of compounds **1** and **2**, which were determined by UV-vis absorption and fluorescence emission spectroscopy, are shown in Fig. 4, and the data are summarized in Table 1. As shown in Fig. 4, **1** and **2** display

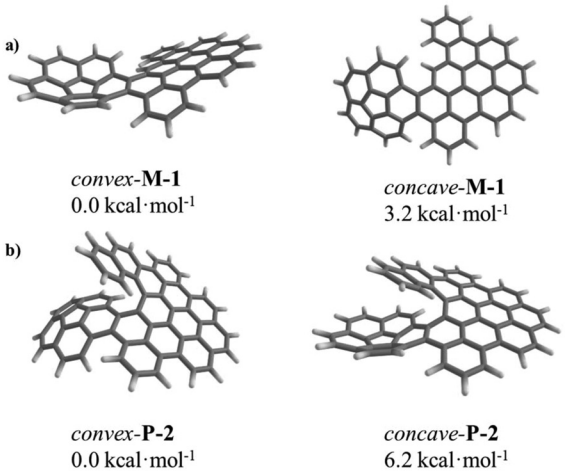

Fig. 3 The terminal rings of the helicene subunits face the *convex* and *concave* π-surfaces of the bowl in theory and their relative free energies were calculated by DFT calculations at the B3LYP/6-31G(d) level of the theory in the gas phase. Free energy is thermally corrected and expressed in kcal mol^{-1}. *t*-Bu groups are omitted for clarity.

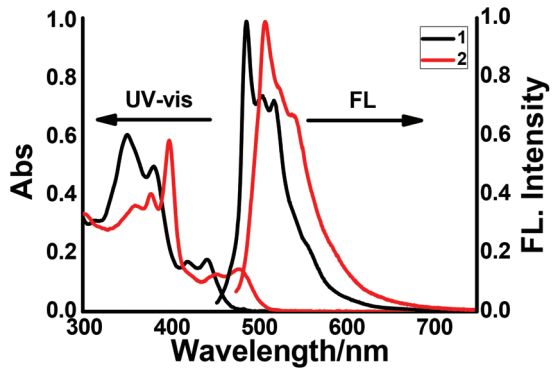

Fig. 4 UV-vis and emission spectra of **1** and **2** were recorded in chloroform solution at room temperature. (All spectra were collected in 1.0 × 10^{-5} M chloroform.)

similar absorption and emission contours. For **1**, obvious absorption bands were observed in a range of 300–490 nm, with the sharpest absorption peak observed at 350 nm, and two moderate absorption peaks observed at 420 and 442 nm. Notably, the absorption bands of **2** display redshifts, with the sharpest absorption at 398 nm and two shoulder peaks at 452 and 479 nm. These redshifts could be ascribed to the expanded π-conjugation of **2**. On the other hand, the emission spectra of **1** and **2** display the maximum peaks located at 487 and 508 nm, respectively. In detail, the emission of **2** shows a redshift of 21 nm, as compared with that of **1**. This observation is in line with the absorption result and further confirms the expansion of the conjugated π-system nature in **2**. Additionally, the photoluminescence quantum yields (Φ_F) of **1** and **2** were determined to be 34% and 22%, respectively. The fluorescence lifetimes (τ) of **1** and **2** were determined to be 12.63 ns and 9.77 ns by single-exponential decay fitting (Fig. S15†), respectively.

Table 1 Absorption and emission data for **1** and **2**

	λ_{abs} [a,b] [nm]	$E_{g(opt)}$ [c] [eV]	λ_{em} [a,d] [nm]	Stokes shift [nm]
1	350	2.53	487	137
2	398	2.36	508	110

[a] λ_{abs} and fluorescence were measured in chloroform (1.0×10^{-5} M) at room temperature. [b] Absorption maximum at the longest wavelength. [c] Estimated from absorption onset, $E_{g(opt)} = 1240/\lambda_{onest}$. [d] Emission maximum ($\lambda_{ex}$ = 360 nm for **1** and 408 nm for **2**).

To better investigate the spectroscopic properties of **1** and **2**, a time-dependent density functional theory (TD-DFT) study was performed at the B3LYP/6-31G(d)/PCM level based on the crystal structures of **1** and **2**. As shown in the top panel of Fig. 5, in the case of **1**, the frontier-molecular-orbital result indicates that the LUMO is localized at all molecules, while the LUMO for **2** is much more localized at the PAH domain. However, the HOMO plots of **1** and **2** are strongly delocalized on the PAH domain. Basically, the energy of the HOMO in **2** increased but the energy of the LUMO decreased, as compared with those of **1**, leading to a decrease of the HOMO–LUMO gap. Additionally, the calculated HOMO–LUMO gaps for **1** and **2** are 3.04 eV and 2.85 eV, respectively, matching with the experimental values of 2.53 eV for **1** and 2.36 eV for **2**. These calculations are in agreement with the experimental bathochromic shift of absorption for **2** with respect to **1**.

The energy diagrams of the dominant excitation are shown in the bottom panel of Fig. 5. TD-DFT calculations confirm the origin of the spectral shifts of **1** and **2**, respectively. In the case of **1**, the absorption band at 442 nm is characterized by the pure HOMO → LUMO transition (f = 0.2402, λ_{calc} = 462 nm), and the absorption band at 420 nm is assigned to a large contribution of the HOMO → LUMO+1 transition and a small contribution of the HOMO−1 → LUMO transition (f = 0.2109, λ_{calc} = 431 nm) (Table S4†). For **2**, the absorption band at 479 nm is attributed to the pure HOMO → LUMO transition (f = 0.3014, λ_{calc} = 499 nm). On the other hand, the absorption band at 452 nm comes from two degenerate excited states from a large contribution of the HOMO → LUMO+1 transition and a small contribution of the HOMO → LUMO+2 transition (f = 0.1055, λ_{calc} = 438 nm) (Table S5†). Furthermore, the HOMO and LUMO also can be considered as a pair of π and π*-molecular orbitals.[4i] Therefore, the absorption appearing at 442 nm for **1** and 479 nm for **2** can be attributed to the π–π* transition, which further reflects the expanded π-conjugation in these nanographenes.

Subsequently, on the basis of the crystal structures, the local aromaticity of the individual rings in **1** and **2** was analysed using the average nucleus-independent chemical shift ($NICS(1)_{ZZ}$)[15] (Fig. 6 and Tables S7, 8†). For the corannulene unit, the $NICS(1)_{ZZ}$ values for the central five-membered ring are positive (13.35 for **1** and 13.45 for **2**, green numbers), whereas those for all the benzene rings are negative. These values strongly suggested that the five-membered ring possesses substantial antiaromatic characteristics, whereas the benzene rings are all aromatic. For the PAH domains, the central benzene rings have small $NICS(1)_{ZZ}$ values of −1.76 for **1** and −1.61 for **2** (blue numbers), indicating the nonaromaticity of the central benzene rings, similar to our previous observations for corannulene based dibenzocoronene.[9] Furthermore, three benzene rings in **1** exhibit medium $NICS(1)_{ZZ}$ values (−5.72, −4.41 and −6.54, red numbers) and four benzene rings in **2** show medium $NICS(1)_{ZZ}$ values (−2.65, −4.20, −3.08 and −3.76, red numbers), revealing that these benzene rings in **1** and **2** show low aromaticity, while other benzene rings have large $NICS(1)_{ZZ}$ values, suggesting the aromaticity of these benzene rings. Moreover, the plots of anisotropy of the induced current density (ACID)[16] reveal the clockwise (diamagnetic) ring currents at the peripheries of corannulene and PAH domains (Fig. S21†), which is an indicator

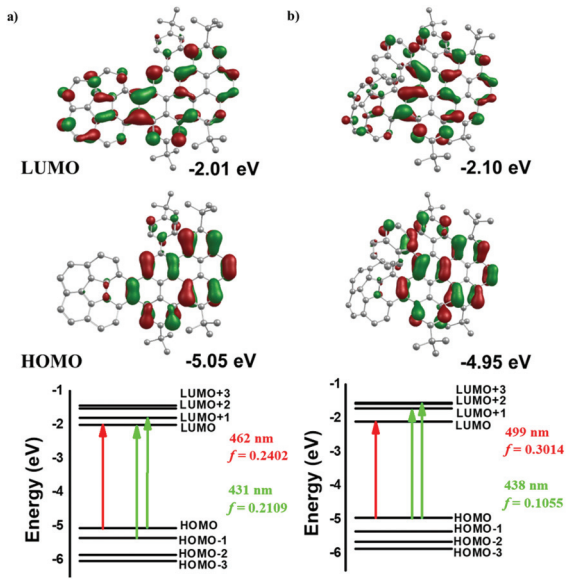

Fig. 5 LUMO (top) and HOMO (middle) energy density and energy diagrams (bottom) of **1** (a) and **2** (b) were calculated by TD-DFT at the B3LYP/6-31G(d)/PCM level. The values of f represent the oscillator strengths.

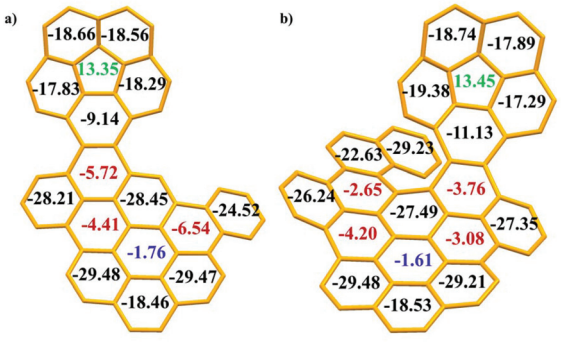

Fig. 6 The average of $NICS(1)_{ZZ}$ values of **1** (a) and **2** (b) were calculated at the GIAO-B3LYP/6-311+G(2d,p)/PCM level based on the crystal structures of **1** and **2**. Hydrogen atoms and *t*-Bu groups are omitted for clarity.

of aromaticity. The anticlockwise (paramagnetic) ring currents at the five-membered rings suggested the antiaromaticity. The plots of ACID are in agreement with NICS(1)$_{ZZ}$ calculations.

The presence of enantiomers in **1** and **2** motivated us to separate their stereoisomers. However, according to DFT calculations, the helix inversion barrier of **1** (4.7 kcal mol^{-1}) (Fig. S19†) is similar to that of pristine [4] helicene (4.1 kcal mol^{-1}),[17] and is small enough for inversion at ambient temperature, suggesting that full chiral resolution of **1** would be unfeasible. For **2**, the helix inversion barrier should be higher than that of pristine [7] helicene (42.0 kcal mol^{-1}),[18] implying that the racemization process is more difficult. So, the chiral resolution of **2** was achieved using an HPLC system equipped with a COSMOSIL Cholester column (eluent : DCM/methanol = 70/30, 2.0 mL min^{-1}). Two distinct peaks were detected (Fig. S14†), corresponding to the two enantiomers of **2**, and they existed at a ratio of 50 : 50. The CD spectra of the two isolated fractions displayed mirror symmetry, indicating that they are enantiomers with opposite helicity (Fig. 7a). The simulated CD spectra of **P-2** and **M-2** were in good agreement with the experimental results (Fig. 7a and b). Accordingly, the first peak and the second peak are assigned to **P-2** and **M-2**, respectively (Fig. S14†). Moreover, **P-2** and **M-2** exhibit circularly polarized luminescence (CPL) activities. The CPL spectra of **P-2** and **M-2** are mirror images. The value of the luminescence dissymmetry factor ($|g_{lum}|$) was about 4.3×10^{-4} (Fig. 7c), which is typically of an order of 10^{-5} to 10^{-3} for small organic molecules.[19]

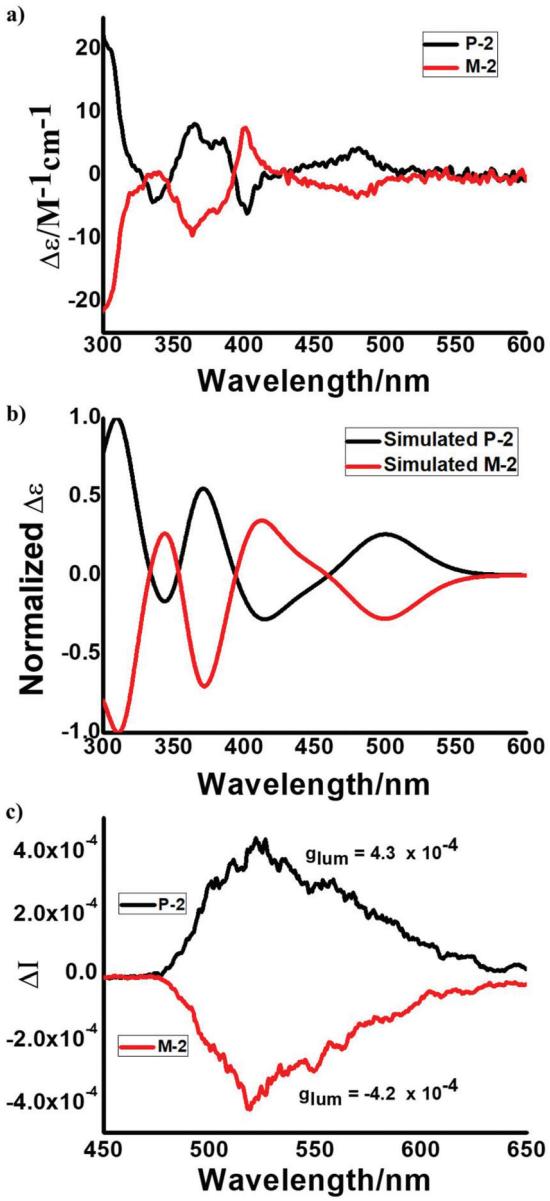

Fig. 7 (a) Experimental CD spectra of **P-2** (black solid line) and **M-2** (red solid line). (b) Simulated CD spectra of **P-2** (black solid line) and **M-2** (red solid line) were conducted by TD-DFT at the B3LYP/6-31G(d)/PCM level. (c) CPL spectra of **P-2** and **M-2**. (All spectra were collected at 1.0×10^{-5} M in chloroform.)

Conclusions

In conclusion, we have achieved the concise bottom-up synthesis of π-conjugated distorted corannulene-PAH hybrids **1** and **2** containing helical motifs and uncovered their structural features. X-ray crystallographic analyses revealed that **1** and **2** are in a *convex* conformation and they adopt a head-to-end layered orientation. Particularly, in the case of **1**, the antiparallel dimer stacking leads to a double-layer and the corannulene units display uniform directions along the crystallographic *a* axis, while the propagation of the double-layer reveals face-to-face stackings along the crystallographic *b* axis. For **2**, the corannulene units display an alternate upside-down orientation along the crystallographic *c* axis and two molecules adopt stackings of antiparallel orientation, in which the bowl-openings of the corannulene units show a uniform direction along the crystallographic *b* axis. Furthermore, the theoretical calculations showed that *convex*-**1** and *convex*-**2** are more stable by 3.2 kcal mol^{-1} and 6.2 kcal mol^{-1}, in comparison with *concave*-**1** and *concave*-**2**, respectively. The enantiomers of **2** were separated by chiral HPLC, and the chirality of thus obtained two fractions of **2** was identified on the basis of their CD spectra supported by TD-DFT calculations. Furthermore, challenges in terms of synthesizing large π-extended corannulene-based chirality materials and developing their practical optoelectronic applications are the topics of ongoing work in our laboratory.

Conflicts of interest

There are no conflicts to declare.

Acknowledgements

We acknowledge the financial support from the National Natural Science Foundation of China (21971020 and 21672026) and Beijing Natural Science Foundation (2212008).

References

1 (*a*) Y. T. Wu and J. S. Siegel, Aromatic Molecular-Bowl Hydrocarbons: Synthetic Derivatives, Their Structures, and Physical Properties, *Chem. Rev.*, 2006, **106**, 4843–4867; (*b*) V. M. Tsefrikas and L. T. Scott, Geodesic Polyarenes by Flash Vacuum Pyrolysis, *Chem. Rev.*, 2006, **106**, 4868–4884; (*c*) A. Narita, X.-Y. Wang, X. Feng and K. Müllen, New advances in nanographene chemistry, *Chem. Soc. Rev.*, 2015, **44**, 6616–6643; (*d*) R. Chen, R.-Q. Lu, P.-C. Shi and X.-Y. Cao, Corannulene derivatives for organic electronics: From molecular engineering to applications, *Chin. Chem. Lett.*, 2016, **27**, 1175–1183; (*e*) J. Shi, Y. Li and Y. Li, Aryne multifunctionalization with benzdiyne and benztriyne equivalents, *Chem. Soc. Rev.*, 2017, **46**, 1707–1719; (*f*) M. Rickhaus, M. Mayor and M. Juráček, Chirality in curved polyaromatic systems, *Chem. Soc. Rev.*, 2017, **46**, 1643–1660; (*g*) Q. Xu, C. Wang, D. Zheng, Y. Wang, X. Chen, D. Sun and H. Jiang, A quadruple helicene with a rubicene core: synthesis, structural analyses and properties, *Sci. China: Chem.*, 2021, **64**, 590–598.

2 A. M. Butterfield, B. Gilomen and J. S. Siegel, Kilogram-Scale Production of Corannulene, *Org. Process Res. Dev.*, 2012, **16**, 664–676.

3 (*a*) T. Hayama, K. K. Baldridge, Y.-T. Wu, A. Linden and J. S. Siegel, Steric Isotope Effects Gauged by the Bowl-Inversion Barrier in Selectively Deuterated Pentaarylcorannulenes, *J. Am. Chem. Soc.*, 2008, **130**, 1583–1591; (*b*) C. Bruno, R. Benassi, A. Passalacqua, F. Paolucci, C. Fontanesi, M. Marcaccio, E. A. Jackson and L. T. Scott, Electrochemical and Theoretical Investigation of Corannulene Reduction Processes, *J. Phys. Chem. B*, 2009, **113**, 1954–1962; (*c*) K. Kawasumi, Q. Zhang, Y. Segawa, L. T. Scott and K. Itami, A grossly warped nanographene and the consequences of multiple odd-membered-ring defects, *Nat. Chem.*, 2013, **5**, 739–744; (*d*) K. Kato, Y. Segawa, L. C. Scott and K. Itami, Synthesis, Properties, and Packing Structures of Corannulene-Based p-Systems Containing Heptagons, *Chem. – Asian J.*, 2015, **10**, 1635–1639; (*e*) V. Rajeshkumar, Y. T. Lee and M. C. Stuparu, Corannulenecarbaldehyde: High-Yielding Synthesis by Rieche Formylation and Facile Access to a Variety of Corannulene Derivatives, *Eur. J. Org. Chem.*, 2016, 36–40; (*f*) Z. Lin, C. Li, D. Meng, Y. Li and Z. Wang, Hybrid Corannulene–Perylene Dyes: Facile Synthesis and Optoelectronic Properties, *Chem. – Asian J.*, 2016, **11**, 2695–2699.

4 (*a*) M. Yanney, F. R. Fronczek and A. Sygula, A 2: 1 Receptor/C_{60} Complex as a Nanosized Universal Joint, *Angew. Chem., Int. Ed.*, 2015, **54**, 11153–11156; (*b*) A. K. Dutta, A. Linden, L. Zoppi, K. K. Baldridge and J. S. Siegel, Extended Corannulenes: Aromatic Bowl/Sheet Hybridization, *Angew. Chem., Int. Ed.*, 2015, **54**, 10792–10796; (*c*) T. Fujikawa, D. V. Preda, Y. Segawa, K. Itami and L. T. Scott, Corannulene-Helicene Hybrids: Chiral π–Systems Comprising Both Bowl and Helical Motifs, *Org. Lett.*, 2016, **18**, 3992–3995; (*d*) K. G. U. R. Kumarasinghe, F. R. Fronczek, H. U. Valle and A. Sygula, Bis-corannulenoanthracene: An Angularly Fused Pentacene as a Precursor for Barrelene-Tethered Receptors for Fullerenes, *Org. Lett.*, 2016, **18**, 3054–3057; (*e*) Y. Tokimaru, S. Ito and K. Nozaki, Synthesis of Pyrrole-Fused Corannulenes: 1,3-Dipolar Cycloaddition of Azomethine Ylides to Corannulene, *Angew. Chem., Int. Ed.*, 2017, **56**, 15560–15564; (*f*) K. Kato, Y. Segawa, L. T. Scott and K. Itami, A Quintuple [6] Helicene with a Corannulene Core as a C 5-Symmetric Propeller-Shaped p-System, *Angew. Chem., Int. Ed.*, 2018, **57**, 1337–1341; (*g*) F. Huang, L. Ma, Y. Che, H. Jiang, X. Chen and Y. Wang, Corannulene-Based Coordination Cage with Helical Bias, *J. Org. Chem.*, 2018, **83**, 733–739; (*h*) W. Sun, Y. Wang, L. Ma, L. Zheng, W. Fang, X. Chen and H. Jiang, Self-Assembled Carcerand-like Cage with a Thermoregulated Selective Binding Preference for Purification of High-Purity C_{60} and C_{70}, *J. Org. Chem.*, 2018, **83**, 14667–14675; (*i*) J. M. Fernández-García, P. J. Evans, S. M. Rivero, I. Fernández, D. García-Fresnadillo, J. Perles, J. Casado and N. Martín, π–Extended Corannulene-Based Nanographenes: Selective Formation of Negative Curvature, *J. Am. Chem. Soc.*, 2018, **140**, 17188–17196; (*j*) W. Sun, L. Ye, J. Liu, L. Zheng, W. Guo, S. Han, C. Shao and H. Jiang, Self-Assembled of Corannulene-Based Molecular Cage with Fullerenes as Template, *Chin. J. Org. Chem.*, 2019, **39**, 2867–2874; (*k*) E. M. Muzammil, D. Halilovic and M. C. Stuparu, Synthesis of corannulene-based nanographenes, *Commun. Chem.*, 2019, **2**, 58–70; (*l*) A. K. Rogachev, Y. Zhu, Z. Zhou, S. Liu, Z. Wei and M. A. Petrukhina, Dimerization of indenocorannulene radicals: imposing stability through increasing strain and curvature, *Org. Chem. Front.*, 2020, **7**, 3591–3598; (*m*) Q. Xu, C. Wang, D. Zheng, J. He, Y. Wang, X. Chen and H. Jiang, A Distorted Hybrid Corannulene-Dibenzobistetracene, *J. Org. Chem.*, 2021, **86**, DOI: 10.1021/acs.joc.0c03065.

5 (*a*) B. M. Schmidt, S. Seki, B. Topolinski, K. Ohkubo, S. Fukuzumi, H. Sakurai and D. Lentz, Electronic Properties of Trifluoromethylated Corannulenes, *Angew. Chem., Int. Ed.*, 2012, **51**, 11385–11388; (*b*) R.-Q. Lu, W. Xuan, Y.-Q. Zheng, Y.-N. Zhou, X.-Y. Yan, J.-H. Dou, R. Chen, J. Pei, W. Weng and X.-Y. Cao, A corannulene-based donor–acceptor polymer for organic field-effect transistors, *RSC Adv.*, 2014, **4**, 56749–56755; (*c*) R.-Q. Lu, Y.-N. Zhou, X.-Y. Yan, K. Shi, Y.-Q. Zheng, M. Luo, X.-C. Wang, J. Pei, H. Xia, L. Zoppi, K. K. Baldridge, J. S. Siegel and X.-Y. Cao, Thiophene-fused bowl-shaped polycyclic aromatics with a dibenzo[a,g]corannulene core for organic field-effect transistors, *Chem. Commun.*, 2015, **51**, 1681–1684; (*d*) Y. Wang, Y. Li, W. Zhu, J. Liu, X. Zhang, R. Li, Y. Zhen, H. Dong and W. Hu, Co-crystal engineering: a novel method to obtain one-dimensional (1D) carbon nanocrystals of corannulene–fullerene by a solution process, *Nanoscale*, 2016, **8**, 14920–14924; (*e*) K. Shoyama, D. Schmidt, M. Mahl and F. Würthner, Electron-Poor Bowl-Shaped Polycyclic Aromatic Dicarboximides: Synthesis, Crystal Structures, and Optical and Redox Properties, *Org. Lett.*, 2017, **19**, 5328–5331; (*f*) R.-Q. Lu, Y. Liu, S. Wu, M. Saha, H. Qu, R. Chen, L.-L. Yang, X.-Y. Wang, Y. Wang, W. Weng, Y. Zhao and X.-Y. Cao, Impacts of

Stereoisomerism on Molecular Packing and Charge Transport of Imide-Fused Corannulene Derivatives, *Cryst. Growth Des.*, 2018, **18**, 4240–4244; (*g*) D. Meng, G. Liu, C. Xiao, Y. Shi, L. Zhang, L. Jiang, K. K. Baldridge, Y. Li, J. S. Siegel and Z. Wang, Corannurylene Pentapetalae, *J. Am. Chem. Soc.*, 2019, **141**, 5402–5408; (*h*) G. Gao, M. Chen, J. Roberts, C. Xiao, G. Zhang, S. Parkin, C. Risko and L. Zhang, Rational Functionalization of a C_{70} Buckybowl To Enable a C_{70}: Buckybowl Cocrystal for Organic Semiconductor Applications, *J. Am. Chem. Soc.*, 2020, **142**, 2460–2470.

6 H.-A. Lin, Y. Sato, Y. Segawa, T. Nishihara, N. Sugimoto, L. T. Scott, T. Higashiyama and K. Itami, A Water-Soluble Warped Nanographene: Synthesis and Applications for Photoinduced Cell Death, *Angew. Chem., Int. Ed.*, 2018, **57**, 2874–2878.

7 (*a*) M. Yanney, F. R. Fronczek, W. P. Henry, D. J. Beard and A. Sygula, Cyclotrimerization of Corannulyne: Steric Hindrance Tunes the Inversion Barriers of Corannulene Bowls, *Eur. J. Org. Chem.*, 2011, 6636–6639; (*b*) V. Rajeshkumar and M. C. Stuparu, A photochemical approach to aromatic extension of the corannulene nucleus, *Chem. Commun.*, 2016, **52**, 9957–9960.

8 Y. Wang, O. Allemann, T. S. Balaban, N. Vanthuyne, A. Linden, K. K. Baldridge and J. S. Siegel, Chiral Atropisomeric Indenocorannulene Bowls: Critique of the Cahn–Ingold–Prelog Conception of Molecular Chirality, *Angew. Chem., Int. Ed.*, 2018, **57**, 6470–6474.

9 Q. Xu, C. Wang, Y. Zhao, D. Zheng, C. Shao, W. Guo, X. Deng, Y. Wang, X. Chen, J. Zhu and H. Jiang, Tuning the Properties of Corannulene-Based Polycyclic Aromatic Hydrocarbons by Varying the Fusing Positions of Corannulene, *Org. Lett.*, 2020, **22**, 7397–7402.

10 J. Mack, P. Vogel, D. Jones, N. Kaval and A. Sutton, The development of corannulene-based blue emitters, *Org. Biomol. Chem.*, 2007, **5**, 2448–2452.

11 H.-J. Zhao, Z.-Z. Zhou, Y. Zhang, X. Su, X.-M. Chen and Y.-M. Liang, Visible-light-mediated borylation of aryl and alkyl halides with a palladium complex, *Org. Biomol. Chem.*, 2020, **18**, 4390–4394.

12 M. J. Fuchter, J. Schaefer, D. K. Judge, B. Wardzinski, M. Weimar and I. Krossing, [7]-Helicene: a chiral molecular tweezer for silver(I) salts, *Dalton Trans.*, 2012, **41**, 8238–8241.

13 J. C. Hanson and C. E. Norman, The crystal and molecular structure of corannulene, $C_{20}H_{10}$, *Acta Crystallogr., Sect. B: Struct. Sci.*, 1976, **32**, 1147–1153.

14 L. T. Scott, M. M. Hashemi and M. S. Bratcher, Corannulene Bowl-to-Bowl Inversion Is Rapid at Room Temperature, *J. Am. Chem. Soc.*, 1992, **114**, 1920–1921.

15 (*a*) R. Herges and D. Geuenich, Delocalization of Electrons in Molecules, *J. Phys. Chem. A*, 2001, **105**, 3214–3220; (*b*) D. Geuenich, K. Hess, F. Kohler and R. Herges, Anisotropy of the Induced Current Density (ACID), a General Method To Quantify and Visualize Electronic Delocalization, *Chem. Rev.*, 2005, **105**, 3758–3772; (*c*) J. Z. Dobrowolski and P. F. J. Lipiński, On splitting of the NICS(1) magnetic aromaticity index, *RSC Adv.*, 2016, **6**, 23900–23904; (*d*) M. Antić, B. Furtula and S. Radenković, Aromaticity of Nonplanar Fully Benzenoid Hydrocarbons, *J. Phys. Chem. A*, 2017, **121**, 3616–3626.

16 (*a*) E. Steiner, P. W. Fowler and L. W. Jenneskens, Counter-Rotating Ring Currents in Coronene and Corannulene, *Angew. Chem., Int. Ed.*, 2001, **40**, 362–366; (*b*) Y. Morita, A. Ueda, S. Nishida, K. Fukui, T. Ise, D. Shiomi, K. Sato, T. Takui and K. Nakasuji, Curved Aromaticity of a Corannulene-Based Neutral Radical: Crystal Structure and 3 D Unbalanced Delocalization of Spin, *Angew. Chem., Int. Ed.*, 2008, **47**, 2035–2038; (*c*) S. N. Spisak, J. Li, A. Y. Rogachev, Z. Wei, O. Papaianina, K. Amsharov, A. V. Rybalchenko, A. A. Goryunkov and M. A. Petrukhina, From Corannulene to Indacenopicene: Effect of Carbon Framework Topology on Aromaticity and Reduction Limits, *Organometallics*, 2016, **35**, 3105–3111; (*d*) T. K. Dickens and R. B. Mallion, Topological Ring Currents and Bond Currents in Some Neutral and Anionic Altans and Iterated Altans of Corannulene and Coronene, *J. Phys. Chem. A*, 2018, **122**, 7666–7678.

17 K. Kato, Y. Segawa and K. Itami, Symmetric Multiple Carbohelicenes, *Synlett*, 2019, **30**, 370–377.

18 (*a*) X.-Y. Wang, X.-C. Wang, A. Narita, M. Wagner, X.-Y. Cao, X. Feng and K. Müllen, Synthesis, Structure, and Chiroptical Properties of a Double [7]Heterohelicene, *J. Am. Chem. Soc.*, 2016, **138**, 12783–12786; (*b*) K. Kato, Y. Segawa and K. Itami, Symmetric Multiple Carbohelicenes, *Synlett*, 2019, **30**, 370–377.

19 (*a*) E. M. Sánchez-Carnerero, A. R. Agarrabeitia, F. Moreno, B. L. Maroto, G. Muller, M. J. Ortiz and S. de la Moya, Circularly Polarized Luminescence from Simple Organic Molecules, *Chem. – Eur. J.*, 2015, **21**, 13488–13500; (*b*) M. Li, W.-B. Lin, L. Fang and C.-F. Chen, Recent Progress on Circularly Polarized Luminescence of Chiral Organic Small Molecules, *Acta Chim. Sin.*, 2017, **75**, 1150–1163; (*c*) H. Tanaka, Y. Inoue and T. Mori, Circularly Polarized Luminescence and Circular Dichroisms in Small Organic Molecules: Correlation between Excitation and Emission Dissymmetry Factors, *ChemPhotoChem*, 2018, **2**, 386–402; (*d*) D. Zheng, L. Zheng, C. Yu, Y. Zhan, Y. Wang and H. Jiang, Significant Enhancement of Circularly Polarized Luminescence Dissymmetry Factors in Quinoline Oligoamide Foldamers with Absolute Helicity, *Org. Lett.*, 2019, **21**, 2555–2559; (*e*) W.-L. Zhao, M. Li, H.-Y. Lu and C.-F. Chen, Advances in helicene derivatives with circularly polarized luminescence, *Chem. Commun.*, 2019, **55**, 13793–13803; (*f*) D. Zheng, C. Yu, L. Zheng, Y. Zhan and H. Jiang, Absolute control of helicity at the C-termini in quinoline oligoamide foldamers by chiral oxazolylaniline moieties, *Chin. Chem. Lett.*, 2020, **31**, 673–676; (*g*) H. Kubo, T. Hirose, T. Nakashima, T. Kawai, J. Hasegawa and K. Matsuda, Tuning Transition Electric and Magnetic Dipole Moments: [7]Helicenes Showing Intense Circularly Polarized Luminescence, *J. Phys. Chem. Lett.*, 2021, **12**, 686–695.

